Comparison of ultrashort-pulse frequency-resolved-optical-gating traces for three common beam geometries

K. W. DeLong and Rick Trebino

Combustion Research Facility, Sandia National Laboratories, Livermore, California 94551

Daniel J. Kane

Southwest Sciences, Inc., 1570 Pacheco Street, Suite E-11, Santa Fe, New Mexico 87501

Received August 20, 1993; revised manuscript received March 21, 1994

We recently introduced frequency-resolved optical gating (FROG), a technique for measuring the intensity and phase of an individual, arbitrary, ultrashort laser pulse. FROG can use almost any instantaneous optical nonlinearity, with the most common geometries being polarization gate, self-diffraction, and second-harmonic generation. The experimentally generated FROG trace is intuitive, visually appealing, and can yield quantitative information about the pulse parameters (such as temporal and spectral width and chirp). However, the qualitative and the quantitative features of the FROG trace depend strongly on the geometry used. We compare the FROG traces for several common ultrashort pulses for these three common geometries and, where possible, develop scaling rules that allow one to obtain quantitative information about the pulse directly from the experimental FROG trace. We illuminate the important features of the various FROG traces for transform-limited, linearly chirped, self-phase modulated, and nonlinearly chirped pulses, pulses with simultaneous linear chirp and self-phase modulation, and pulses with simultaneous linear chirp and cubic phase distortion, as well as double pulses, pulses with phase jumps, and pulses with complex intensity and phase substructure.

INTRODUCTION

The measurement of the intensity and phase evolution of ultrashort pulses is a problem that, for many years, defied solution. Techniques such as autocorrelation[1,2] and interferometric autocorrelation[3,4] require *a priori* assumptions about the nature of the pulse, while methods that do not require such assumptions are complex and cannot operate on a single shot.[5–9] However, the recently developed technique of frequency-resolved optical gating[10–12] (FROG) permits the complete recovery of the pulse intensity and phase evolution without assumptions on a single-shot basis and with a simple apparatus. This technique produces an experimental trace (hereafter referred to as the FROG trace) that is related to the spectrogram[13–15] of the pulse, from which the complete complex electric field of the pulse can be determined by a simple and robust iterative algorithm.[11,16]

The spectrogram, and hence the FROG trace, is in general intuitive and visually appealing. Indeed, in fields where the spectrogram is commonly used (such as acoustics), such a trace is often preferred to the actual waveform for display.[13–15] Like the FROG trace, the spectrogram is the short-term spectrum of the pulse and generally mirrors the graph of the pulse's instantaneous frequency as a function of time. The use of spectrograms in representing optical pulses was pioneered by Treacy.[17] Other time–frequency representations, such as the Wigner function, have been suggested for use in ultrashort-pulse research,[18,19] but measuring such quantities is significantly more difficult than obtaining a FROG trace.

The complete FROG trace is directly viewable in the laboratory on each laser shot as an image on a two-dimensional camera array. Thus FROG provides immediate visual feedback on all important pulse characteristics, such as pulse length, chirp, self-phase modulation, and spectral width. Knowledge of the type of trace obtained for a given pulse would greatly assist in the alignment of lasers, pulse compressors, and other optical components, as well as in the understanding of the basic physics of the lasers themselves.

The nonlinear mechanism required for generating a FROG trace can result from a variety of processes, the main requirement being that the effect be instantaneous. We have used polarization (Kerr) rotation in a polarization-gate (PG) beam geometry, self-diffraction (SD, three-wave mixing), and second-harmonic generation (SHG). It is possible to use third-harmonic generation, as well as cascaded $\chi^{(2)}$ processes, which then appear as a $\chi^{(3)}$ process. In this paper we concentrate on the PG, SD, and SHG geometries because these geometries have been demonstrated experimentally and are anticipated to be the most useful.

Interestingly, the different types of FROG show nontrivial differences in their traces. PG FROG traces are the most intuitive, and the pulse-retrieval algorithm is most robust in PG FROG.[16] SD FROG traces contain much more structure than PG FROG traces and are therefore slightly more difficult to interpret. SHG FROG

0740-3224/94/091595-14$06.00

contains a temporal ambiguity[10,11,20,21] (a pulse and its time-reversed replica yield identical SHG FROG traces), and therefore SHG FROG traces are always symmetric with respect to delay. As a result one cannot determine the sign of spectral phase distortions and even-order temporal phase distortions (such as linear chirp).

Our purpose in this paper is to compare the characteristics of the FROG traces generated by the various FROG geometries and to present a catalog of theoretical FROG traces, which will assist experimentalists in determining pulse characteristics immediately from the visual data of the FROG trace. We develop scaling rules that allow one to obtain quantitative information about the pulse directly from the FROG trace without the use of the pulse-retrieval algorithm. We also discuss in detail the characteristics of the FROG trace so that, when confronted with a new or previously unseen trace, the researcher may be able to interpret it and have a good idea of what the pulse intensity and phase may be without the use of the iterative algorithm. With the insight provided by this catalog and discussion, FROG becomes a real-time feedback system for essentially all ultrashort-pulse parameters.

We begin with a short discussion of the various FROG geometries and the experimental issues encountered in using them and review the experimental FROG setup. We then introduce the concept of the marginal, a useful quantity generated from the FROG trace, and mention some scaling laws that allow us to derive quantitative information about the pulse directly from the marginals of the FROG trace. We then explore FROG traces for the various geometries in detail, beginning with a transform-limited pulse and followed by traces for pulses with linear chirp, self-phase modulation (SPM), and cubic spectral and temporal phase distortion. We discuss some unique features of FROG for detecting double pulses, showing that the FROG trace measures the relative phase shift of two pulses to within a small fraction of a wavelength even if the pulses are separated by many pulse lengths. We then present the case (applicable to pulse compression) of a self-phase modulated pulse undergoing negative group-velocity dispersion (GVD) as well as a pulse with simultaneous linear chirp and spectral cubic phase distortion. Finally, we show traces for pulses with phase jumps and for pulses with significant random intensity and phase substructure.

TYPES OF FREQUENCY-RESOLVED OPTICAL GATING

The various types of FROG geometry (Fig. 1) are suited to slightly different experimental regimes. Here we shall briefly explore some of the experimental concerns.

In PG FROG[12] the signal is generated by nonlinear Kerr polarization rotation of the probe pulse by the gate pulse. PG FROG is automatically phase matched, which allows for large crossing angles and hence large delay ranges in the single-shot geometry, permitting its use for measuring long pulses. PG FROG does, however, require propagation through a polarizer before the measurement and so may not be suitable for extremely short or ultraviolet pulses. The limiting source of noise in a PG FROG experiment is usually leakage of the probe beam through the crossed polarizers.

SD FROG[10] uses the self-diffracted (also called three-wave or forward four-wave mixing) signal. SD FROG is not phase matched and hence requires a relatively thin nonlinear medium and a small beam-crossing angle. This limits the maximum length of pulse that can be measured with SD FROG in a single-shot geometry. SD FROG therefore appears useful for ultraviolet and extremely short pulses, as it involves minimal propagation through optical components. Light scattered off the sample surface into the signal direction may be the main noise source for this measurement (although using orthogonal polarizations may help in this case).

SHG FROG,[10,11,20–22] which uses the normal second-harmonic autocorrelation signal, is limited in its wavelength range but is useful for low-energy pulses. It is difficult to generate sufficient signal from a third-order nonlinearity for pulses with peak intensities of less than 10^5 W (10 nJ for a 100-fs pulse). Because the signal is generated at a frequency different than that of the input light, scattering is not a problem. However, one is limited in the maximum length of the crystal that one can use because of group-velocity mismatch.

Other FROG geometries, which have not yet been realized experimentally, are possible. Third-harmonic generation will be severely limited in its useful wavelength range but maintains the advantage that scattered light from the fundamental beam will not interfere with the (frequency-tripled) signal beam. Cascaded $\chi^{(2)}$ effects[23] can mimic the functional form of self-diffraction of third-harmonic generation and may have longer effective nonlinear coefficients $\chi^{(3)}_{\text{eff}}$ than usual third-order nonlinearities. They do, however, suffer from a more complicated alignment procedure.

FREQUENCY-RESOLVED-OPTICAL-GATING TRACE

For the single-shot version of FROG, two replicas (which we call the gate and the probe pulses) of the pulse to be measured are focused with a cylindrical lens and crossed

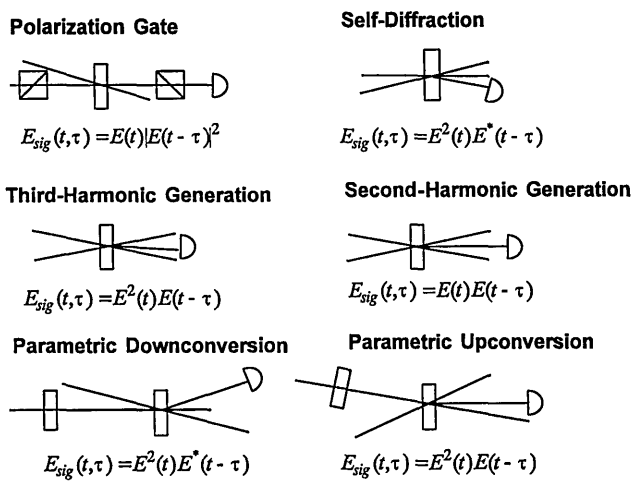

Fig. 1. Schematic of the various experimental geometries for generating FROG traces. The nonlinear mixing signal is spectrally resolved as a function of delay time between the two replicas of the beam to be measured. The parametric conversion geometries use two crystals with a second-order nonlinearity, cascaded to produce an effective third-order nonlinearity.

in a nonlinear-optical medium (see Fig. 1) in the manner of a single-shot autocorrelator. In this fashion relative delay is varied spatially across the medium. In PG FROG the probe, or test, pulse passes through crossed polarizers that are placed on either side of the nonlinear medium. The gain pulse is polarized at roughly a 45° angle to the probe pulse, typically by out-of-plane propagation. The optical Kerr polarization-rotation effect[12] produces a signal field

$$E_{\text{sig}}{}^{\text{PG}}(t, \tau) = E(t)|E(t-\tau)|^2, \tag{1}$$

in which the first factor, $E(t)$, is due to the probe field and the second factor, $|E(t-\tau)|^2$, is due to the gate field. In SD FROG, which is not phase matched, the apparatus is similar, but we use the self-diffracted signal, which has the form

$$E_{\text{sig}}{}^{\text{SD}}(t, \tau) = E^2(t)E^*(t-\tau). \tag{2}$$

In SHG FROG the frequency-doubled light of the autocorrelation forms the signal beam, so that

$$E_{\text{sig}}{}^{\text{SHG}}(t, \tau) = E(t)E(t-\tau). \tag{3}$$

The signal beam is imaged onto the entrance slit of an imaging spectrometer by a spherical lens, where the relative time delay τ between the probe and the gate pulses is parameterized along the slit. The spectrometer disperses the light in a direction perpendicular to the slit, resulting in a two-dimensional image with delay time τ and frequency ω as the axes. The CCD array detects the intensity, so that the FROG trace has the mathematical form

$$I_{\text{FROG}}(\omega, \tau) = \left| \int_{-\infty}^{\infty} \mathrm{d}t E_{\text{sig}}(t, \tau)\exp(i\omega t) \right|^2. \tag{4}$$

The FROG trace is formally equivalent to the spectrogram[13–15] $S_g[\omega, \tau; E(t)]$ of $E(t)$,

$$S_g[\omega, \tau; E(t)] = \left| \int_{-\infty}^{\infty} \mathrm{d}t E(t)g(t-\tau)\exp(i\omega t) \right|^2, \tag{5}$$

where $g(t)$ is a gate function. The gate in a usual spectrogram is typically an independent, simple, and known function, such as a rectangular function or a Gaussian. In FROG, on the other hand, to avoid the need for an independent reference pulse, the pulse itself provides the gate. It is this use of the pulse to gate itself that gives FROG its dynamic range and power. For example, for best results the gate should have a width somewhat, but not too much, shorter than the pulse. This is guaranteed in FROG because the gate is some simple function of the pulse. In addition, an ambiguity is known to exist in the spectrogram (the relative phase of well-separated pulses); but because FROG's gate is always approximately as long as the pulse, this ambiguity does not occur in FROG.[10,11] Thus in some ways FROG is superior to the standard spectrogram.

In PG FROG the gate is a strictly real function—the intensity envelope of the pulse. This leads to FROG traces that are intuitive and visually appealing. In SD FROG the gate is a potentially complex function and thus introduces extra phase (frequency) information into the FROG trace. Thus SD FROG traces, in general, will be more complicated and contain more detail than PG FROG traces. In SHG FROG the gate is simply a replica of the pulse, a fact that introduces a temporal ambiguity into the SHG FROG problem.[21]

A simple visual inspection of the FROG trace provides extensive information about the pulse. The horizontal and the vertical extents of the FROG trace give the temporal and the spectral widths to within an order of unity correction. These notions can be made quantitative through the use of the marginal, which we now discuss.

MARGINALS

Many useful properties of the spectrogram, and hence of the FROG trace, are summarized in the excellent paper by Altes.[15] Probably the most useful for interpreting FROG traces are those relating to the marginals, and we summarize those properties here. The delay marginal is the integral of the FROG trace along the frequency axis:

$$M_\tau(\tau) \equiv \int_{-\infty}^{\infty} \mathrm{d}\omega I_{\text{FROG}}(\omega, \tau), \tag{6}$$

yielding a function of delay only. For PG and SD FROG the delay marginal has the form

$$M_\tau{}^{\text{PG}}(\tau) = M_\tau{}^{\text{SD}}(-\tau) = \int_{-\infty}^{\infty} \mathrm{d}t I(t)I^2(t-\tau). \tag{7}$$

In other words, integrating the FROG trace along the frequency axis yields the third-order intensity autocorrelation. In SHG FROG the delay marginal has the form

$$M_\tau{}^{\text{SHG}}(\tau) = \int_{-\infty}^{\infty} \mathrm{d}t I(t)I(t-\tau), \tag{8}$$

which is the standard second-order intensity autocorrelation of the pulse.

We also define the frequency marginal, which is the integral of the FROG trace along the delay axis and hence a function of frequency only:

$$M_\omega(\omega) \equiv \int_{-\infty}^{\infty} \mathrm{d}\tau I_{\text{FROG}}(\omega, \tau). \tag{9}$$

The form of the frequency marginal is also dependent on the nonlinearity used in creating the FROG trace. For PG FROG it is related to the pulse spectrum and second-order intensity autocorrelation, $A^{(2)}(t)$, of the pulse:

$$M_\omega{}^{\text{PG}}(\omega) = I(\omega) * F\{A^{(2)}(\tau)\}, \tag{10}$$

where $F\{\}$ indicates the Fourier transform and $*$ indicates convolution. In the case of SD FROG the frequency marginal has the form

$$M_\omega{}^{\text{SD}}(\omega) = I(-\omega) * F\{E^2(t) \otimes [E^*(t)]^2\}, \tag{11}$$

where $\otimes$ denotes cross correlation and the superscript asterisk indicates complex conjugation. Equation (11) can be rewritten as

$$M_\omega{}^{\text{SD}}(\omega) = I(-\omega) * I_{\text{SH}}(\omega), \tag{12}$$

where $I(\omega)$ is the spectrum of the pulse and $I_{SH}(\omega)$ is the spectrum of the second harmonic, $E^2(t)$, of the pulse. For SHG FROG the frequency marginal has the simple form

$$M_\omega^{SHG}(\omega) = 2I(\omega) * I(\omega). \tag{13}$$

The mean frequency of the FROG trace at a given delay time τ is often simply related to the instantaneous frequency of the pulse at time t,

$$f(t) = -\frac{1}{2\pi}\frac{d\phi(t)}{dt}, \tag{14}$$

where $\phi(t)$ is the phase of the electric field as a function of time. To quantify this notion, we calculate the first moment of the FROG trace taken at each delay value,

$$\bar{f}(\tau) = \frac{1}{2\pi}\frac{\int_{-\infty}^{\infty} d\omega\,\omega I_{FROG}(\omega, \tau)}{\int_{-\infty}^{\infty} d\omega I_{FROG}(\omega, \tau)}. \tag{15}$$

We call this quantity the first-order delay marginal (FODM). In the next section we develop some scaling laws that allow us to relate the FODM to $f(t)$.

SCALING RULES FOR THE INSTANTANEOUS FREQUENCY

The FROG trace usually provides a good approximation to the instantaneous frequency as a function of time, $f(t)$. This is what gives the FROG technique its visual appeal: one can generally see the manner in which the instantaneous frequency changes during the pulse directly from the FROG trace.

It would be useful if we could obtain quantitative results, such as the amount of linear chirp in a pulse, from a simple visual inspection of its FROG trace. However, the FROG trace does not directly reveal the instantaneous frequency as a function of time. Instead $f(t)$ is scaled or distorted in some usually predictable way. Here we derive some simple relations that allow us to construct scaling laws to relate the information available in the FROG trace to $f(t)$.

The information available in the FROG trace is summarized by the FODM of Eq. (15). (The FODM gives us the slope or curvature of the FROG trace when these concepts are appropriate.) The FODM, being the mean frequency of the FROG trace at delay time τ, should be equal to the center frequency of the signal field, $\Omega_{sig}(\tau)$, at the same delay time τ. We can compute $\Omega_{sig}(\tau)$ analytically and then use a Taylor series expansion to reveal how the various orders of frequency distortion are scaled in the FROG trace.

In PG FROG, with Gaussian pulses, the signal field $E_{sig}(t, \tau)$ is centered at the time[12] $2\tau/3$ (the signal field will be centered at slightly different times for different pulse shapes). In PG FROG the gate is a strictly real function and does not introduce any phase into the signal beam. Therefore the frequency of the signal field when the time delay is τ can be written as

$$\Omega_{sig}^{PG}(\tau) = \omega(^2/_3\,\tau). \tag{16}$$

Expanding this equation in a Taylor series would indicate that the nth-order frequency distortion is scaled in the FROG trace by a factor of $(2/3)^n$.

For SD FROG the relation is more complex. Because the signal pulse is centered at approximately the time $\tau/3$ and the expression for the signal frequency in SD FROG is $\Omega_{sig}^{SD} = 2\omega_p - \omega_g$, the instantaneous frequency of the signal pulse will be $\Omega_{sig}^{SD}(\tau) \approx 2\omega(\tau/3) - \omega(-2\tau/3)$. Expanding $\omega(\tau)$ in a Taylor series, we obtain[10]

$$\Omega_{sig}^{SD}(\tau) = \sum_{n=0}^{\infty}\left[\frac{2-(-2)^n}{3^n}\right]\frac{\omega^{(n)}(0)\tau^n}{n!}, \tag{17}$$

the first few terms of which are

$$\Omega_{sig}^{SD}(\tau) = \omega(0) + \left(\frac{4}{3}\right)\omega^{(1)}(0)\tau - \left(\frac{2}{9}\right)\frac{\omega^{(2)}(0)}{2}\tau^2 + \left(\frac{10}{27}\right)\frac{\omega^{(3)}(0)}{6}\tau^3 + \ldots, \tag{18}$$

where $\omega^{(n)}(0)$ is the nth derivative of $\omega(t)$ evaluated at $t = 0$. The coefficient in the square brackets in Eq. (17) [those in parentheses in Eq. (18)] multiplies the usual Taylor-series terms for $\omega(t)$. When this coefficient is larger than one, the effect of that particular order of phase distortion will be amplified in the SD FROG trace. The coefficients for even orders of frequency distortion (odd orders of phase distortion) are negative. This means that the apparent sign of the phase distortion is reversed in the FROG trace. We give an example of this in the section below on Temporal Cubic Phase.

Similarly, for SHG FROG we see that $\Omega_{sig}^{SHG}(\tau) = \omega(\tau/2) + \omega(-\tau/2)$, and we can expand this in a Taylor series to get

$$\Omega_{sig}^{SHG}(\tau) = \sum_{n=0}^{\infty}\frac{\omega^{(n)}(0)\tau^n}{n!}\left[\left(\frac{1}{2}\right)^n + \left(-\frac{1}{2}\right)^n\right], \tag{19}$$

which has as the first few terms

$$\Omega_{sig}^{SD}(\tau) = 2\omega(0) + \left(\frac{1}{2}\right)\frac{\omega^{(2)}(0)}{2}\tau^2 + \left(\frac{1}{8}\right)\frac{\omega^{(4)}(0)}{24}\tau^4 + \ldots. \tag{20}$$

We see that in SHG FROG the odd-order frequency distortions (even-order phase distortions) such as linear chirp are not apparent in the FROG trace at all. This does not mean that SHG FROG is insensitive to these phase distortions. For example, in the case of linear chirp the SHG FROG trace becomes wider in frequency as the amount of chirp increases, but it does not acquire slope (as in the PG and SD cases), and therefore positive and negative chirp are indistinguishable. Also, for higher-order phase distortions the value of the Taylor series coefficient decreases, reducing the visibility in the SHG FROG trace.

We can use the relations developed above to estimate the quantitative amount of phase distortion from a simple visual inspection of the FROG trace. By measuring the FODM of the FROG trace [and therefore $\Omega_{sig}(\tau)$] we can use the scaling coefficients to deduce the true amount of phase distortion in the pulse. In general this sort of estimation appears to work well as long as only one type of phase distortion is present in the pulse. In general, however, if quantitative results are needed, the safest route is to entrust the recovery of such values to the pulse-retrieval algorithm. This will be discussed in more detail for the various pulses below.

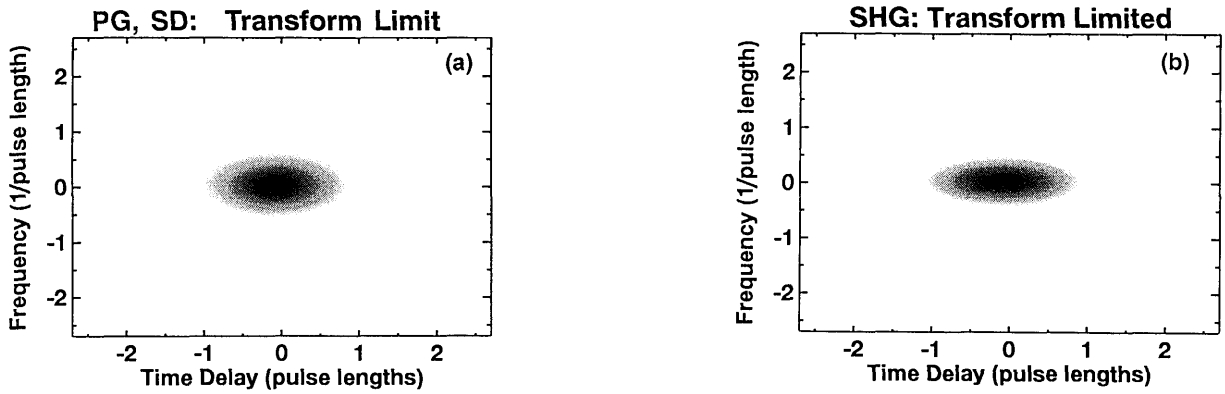

Fig. 2. FROG traces for a Gaussian-shaped transform-limited pulse. The FROG trace for all three geometries are ellipses for this pulse. (a) The PG and the SD FROG traces are identical for this case. (b) The SHG FROG trace is wider in frequency but narrower in delay than the PG and the SD FROG traces. The frequency axis is labeled in linear, not angular, frequency units.

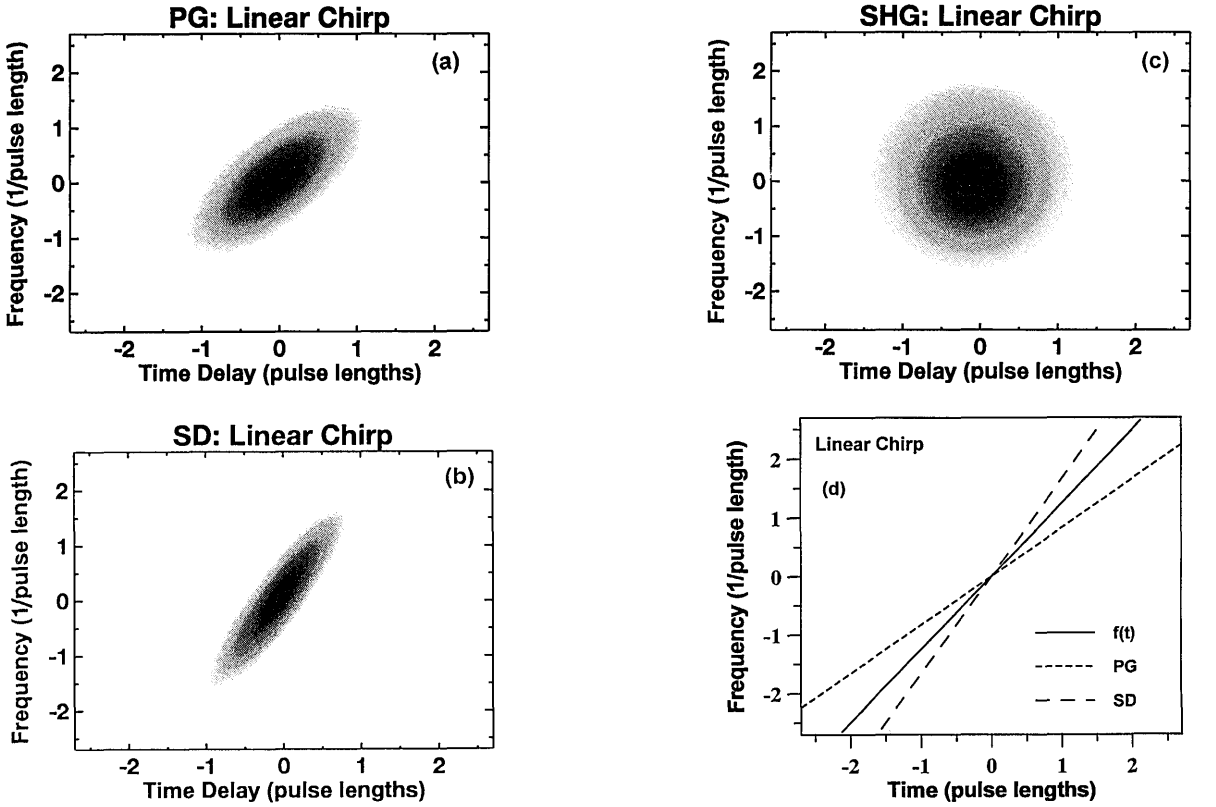

Fig. 3. (a)–(c) FROG traces for a linearly chirped pulse. The linear chirp parameter was chosen to broaden the spectrum by a factor of 3 over the unchirped spectral width. The PG and the SD FROG traces are tilted ellipses, whereas the SHG FROG trace is untilted. The nearly circular form of the SHG FROG trace in this case is an accident of the pulse parameters and scaling of the figure; the trace is, in general, elliptical. (d) Instantaneous frequency as a function of time, $f(t)$, and the FODM's for PG and SD FROG (in SHG FROG the FODM is flat). The FODM essentially measures the slope of the FROG trace. The slope of the SD FROG trace is twice that of the PG FROG trace for a linearly chirped pulse.

TRANSFORM-LIMITED PULSE

As a first example we examine the transform-limited Gaussian pulse (the optical carrier frequency has been removed from all electric fields in this paper),

$$E(t) = \exp(-at^2), \tag{21}$$

which has a FWHM in intensity of

$$\tau_{\mathrm{FW}} = \left[\frac{2\ln(2)}{a}\right]^{1/2} \tag{22}$$

and a spectral width of

$$f_{\mathrm{FWHM}} = \frac{2\ln(2)}{\pi\tau_{\mathrm{FW}}}. \tag{23}$$

The various FROG traces for this pulse are displayed in Fig. 2 (the PG and SD FROG traces are identical for the transform-limited pulse). They appear as an ellipse centered at the origin with major and minor axes along the $\tau = 0$ and $f = 0$ axes. The temporal FWHM of the PG and SD FROG traces at $f = 0$ is 1.22 times wider than the

FWHM of the original pulse, and the spectral FWHM at $\tau = 0$ is 1.73 times wider than the spectral FWHM of the original pulse. In SHG FROG both widths are $\sqrt{2}$ times wider.[24] (Note that although the analytical expression for the FROG trace uses the angular frequency, all FROG traces in this paper use the linear frequency f.)

LINEARLY CHIRPED PULSE

We write the electric-field envelope of a linearly chirped pulse as

$$E(t) = \exp[(-a + ib)t^2]. \tag{24}$$

This pulse has a spectral bandwidth that is increased over the transform limit[25] by $[1 + (b/a)^2]^{1/2}$. Figure 3 shows the FROG traces of a positively chirped pulse, where the chirp parameter b was chosen to triple the spectral bandwidth of the unchirped ($b = 0$) pulse. Note that in such a positively chirped pulse the leading edge of the pulse (negative times) has a lower frequency than the trailing edge of the pulse (positive times), as reflected in the PG and SD FROG traces. Conversely, a pulse with negative chirp leads to a negative slope in the PG and the SD FROG traces. In SHG FROG the sign of the chirp is indeterminate, and the trace exhibits zero slope. [In Fig. 3(c) the SHG FROG trace appears to be circular. This is a coincidence of the pulse parameters and the scaling chosen for the graph. The SHG FROG trace of a linearly chirped pulse is, in general, an ellipse.] This illustrates one of the main disadvantages of SHG FROG: the traces for positive and negative chirp are identical, so that one cannot learn the sign of the chirp from the SHG FROG trace.

The PG and the SD FROG traces closely parallel the $f(t)$ curve, seen in Fig. 3(d). This is because FROG is a time-domain sampling process, like the temporal method of Ref. 26, and therefore inherently measures the frequency as a function of time. Of course, the FROG trace contains full information regarding the pulse in either domain; it simply looks more like the time-domain representation of the pulse than the frequency-domain representation of the pulse.

To obtain a quantitative measure of the chirp directly from the FROG trace, it is necessary to compare the slope of the FROG trace to the slope of the true instantaneous frequency versus time, $f(t)$. To find the slope of the FROG trace, we use the FODM of Eq. (15). The instantaneous frequency as a function of time is calculated from Eq. (14).

Figure 3(d) shows $f(t)$ of the pulse and the PG and the SD FROG FODM's. [the FODM for SHG FROG is flat, as is predicted by Eq. (20).] In PG FROG the slope of the FODM is 2/3 that of $f(t)$. This agrees with Eq. (16), when it is remembered that in linear chirp the instantaneous frequency goes linearly with time. The slope of the FODM in SD FROG is 4/3 that of $f(t)$, as is predicted by the second term of Eq. (18), and has twice the slope as in PG FROG. Thus, by measuring the FODM of the PG or the SD FROG trace, we see that we can accurately determine the amount of chirp in a linearly chirped pulse.

The SHG FROG trace does not acquire any slope for a linearly chirped pulse. However, we can still make an estimate of the amount of chirp by measuring the spectral width of the SHG FROG trace at $\tau = 0$. This width is $\sqrt{2}$ wider than the spectral width of the pulse itself (for Gaussian pulses). There is a drawback to this method, however: in SHG FROG a mere visual inspection of the trace does not reveal whether linear chirp is the dominant phase distortion, in contrast to the case for PG and SD FROG.

SELF-PHASE MODULATION

SPM is an intensity-dependent phase that a pulse may acquire by passing through a Kerr medium such as an optical fiber.[27] The electric field is written as

$$E(t) = \exp[-at^2 + iQ|E(t)|^2]. \tag{25}$$

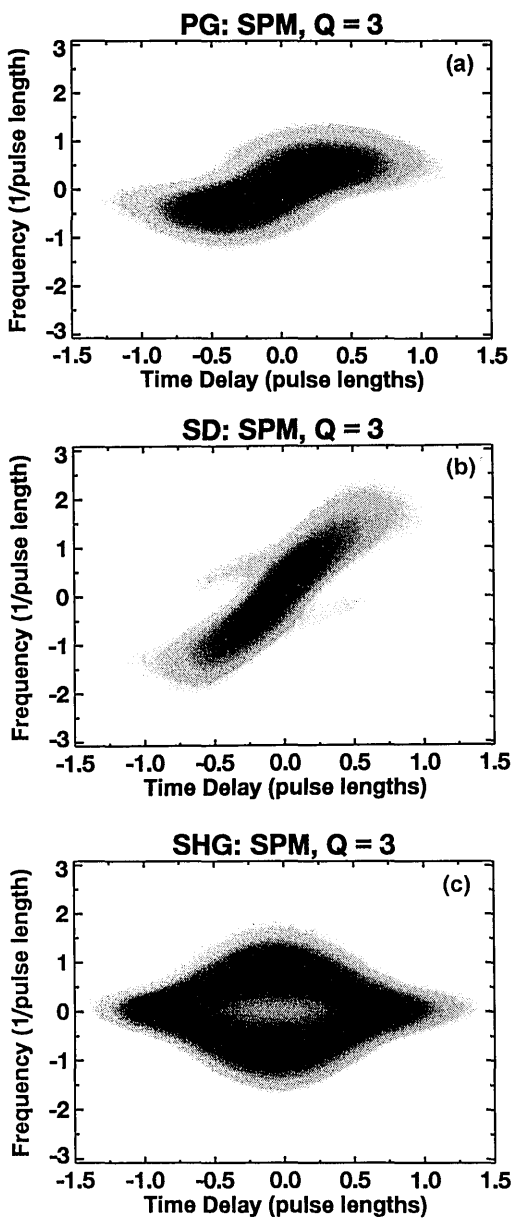

Fig. 4. (a)–(c) FROG traces for a self-phase modulated pulse with $Q = 3$. The PG and the SD FROG traces show the characteristic features of SPM, with lower frequencies generated in the rising edge of the pulse and higher frequencies in the falling edge of the pulse.

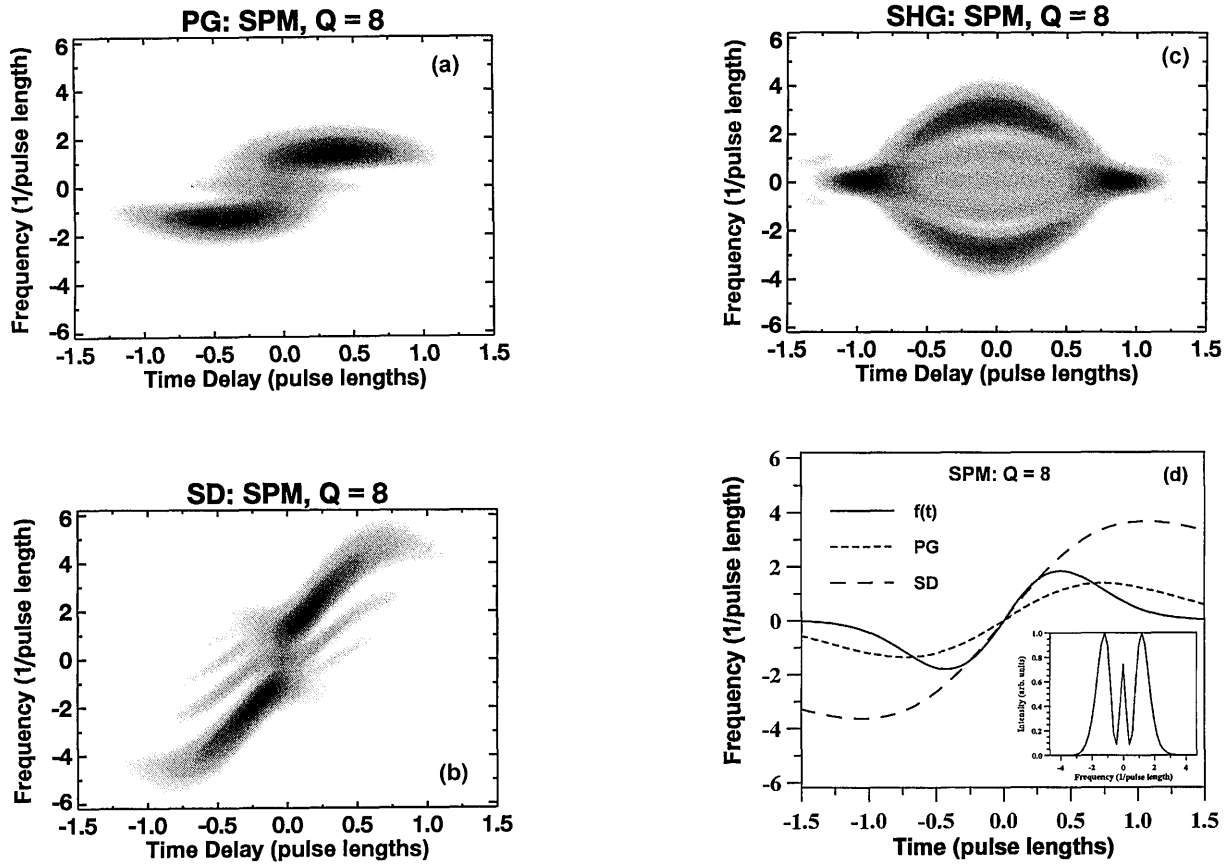

Fig. 5. (a)–(c) FROG traces for a self-phase modulated pulse with $Q = 8$. All the traces exhibit considerable structure. (d) $f(t)$ for the pulse, as well as the FODM for PG and SD FROG traces (the FODM for SHG FROG is flat in this case). Here we see how SD FROG accentuates the features of SPM. The spectrum, seen in the inset, has three peaks, a fact most clearly reflected in the PG FROG trace (a).

For a positive value of Q, lower frequencies are generated in the leading edge of the pulse, while higher frequencies are generated in the trailing edge. In Figs. 4 and 5 we see two cases of self-phase modulated pulses, the first with a moderate amount of SPM, $Q = 3$, and the second with a larger amount of SPM, $Q = 8$.

For the $Q = 3$ case shown in Fig. 4 we see that, while the PG and the SD FROG traces have taken on the characteristic S shape of SPM, the SHG FROG trace is not nearly so intuitive. In Fig. 5 the $Q = 8$ case shows a larger SPM distortion, and the FROG traces exhibit much more structure than the $Q = 3$ case. The detailed structure of the SD FROG traces includes wisplike fringes. This is because the gate pulse in SD FROG is a complex function, rather than real, and thus contributes phase (frequency) to the signal beam. The spectrum of the pulse, plotted as the inset in Fig. 5(d), exhibits three peaks for $Q = 8$. This is reflected clearly in the PG FROG trace but not so strongly in the SD or the SHG FROG traces.

Also in Fig. 5(d) we see the $f(t)$ curve for the pulse, as well as the FODM for PG and SD FROG. Using this information, we can derive scaling laws for pulses with SPM. For PG FROG the FODM is elongated in time by a factor of 1.75 and reduced in magnitude by a factor of 0.75 compared with the analytically derived $f(t)$. If Eq. (16) actually held, these factors would be 1.5 and 1, respectively. In the case of SD FROG we find that the time axis of the FODM is stretched by a factor of ~2.5, while the frequency axis is stretched by a factor of ~2. The FODM of SHG FROG, being identically zero, allows no such comparison.

However, once we know these correction factors, we can estimate the value of Q directly from the PG or the SD FROG trace of a self-phase-modulated pulse. The maximum frequency excursion of $f(t)$ for a pulse of the form of Eq. (25) is $f_{\max} = 0.227Q$. (All frequencies are normalized to the inverse pulse width.) When we include the empirically determined factors mentioned above, we find that the maximum frequency excursion of the FODM, $\bar{f}_{\max}$, is related to the value of Q through $\bar{f}_{\max}{}^{PG} = 0.170Q$ for PG FROG and $\bar{f}_{\max}{}^{SD} = 0.455Q$ for SD FROG.

TEMPORAL CUBIC PHASE

It is also important to be able to characterize higher-order phase distortions, such as cubic phase, and FROG does this. As an example, we consider the sample case of temporal cubic phase in the absence of other distortions, in which case the electric field is written as

$$E(t) = \exp(-at^2 + ict^3). \tag{26}$$

A pulse with this type of chirp was seen experimentally with FROG[28] when a self-phase-modulated pulse was amplified by a narrow-band amplifier. The FROG traces of a pulse with chirp of this form, in which we have used $c = -4/\tau_{FW}{}^3$, are plotted in Fig. 6. In this case the pulse instantaneous frequency has the shape of a parabola, and we see that the FROG trace also closely follows this shape.

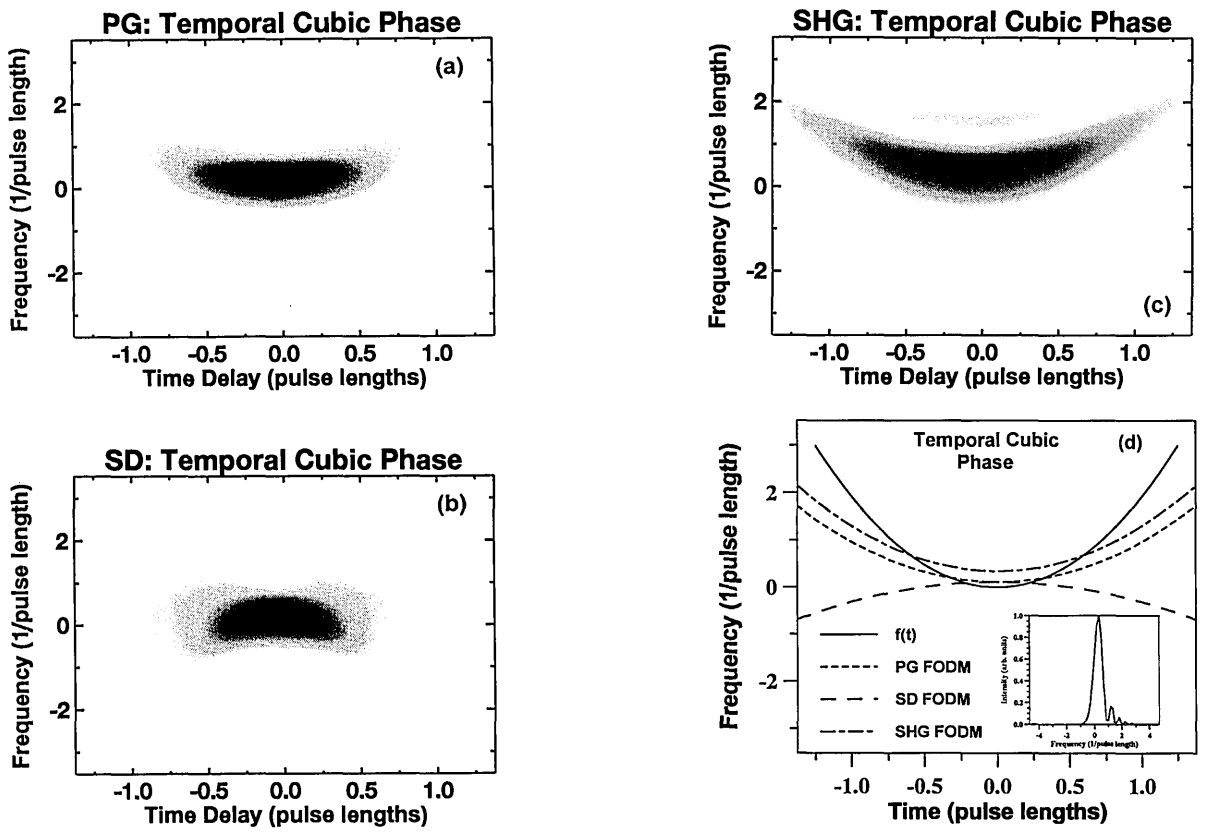

Fig. 6. (a)–(c) FROG traces of a pulse with temporal cubic phase distortion. All the traces exhibit a crescent shape. (d) $f(t)$ for the pulse, as well as the FODM's of the FROG traces. The slope of the SD FROG FODM is negative (see text). The spectrum of this pulse (inset) shows a beating phenomenon, a fact most clearly reflected in the SHG FROG trace.

In a pulse such as this one with positive temporal cubic phase, the leading and the trailing edges of the pulse have a higher frequency than the center of the pulse. The frequency spectrum of this pulse also is plotted as the inset in Fig. 6(d). There is a beating effect at the higher frequencies because these frequencies are present at two different times in the pulse, as is suggested by the FROG trace and the $f(t)$ curve.

Once again we can extract quantitative information directly from the FROG trace. Figure 6(d) shows the FODM's of the three FROG traces as well as the $f(t)$ curve. In PG FROG the curvature of the FODM is found to be 4/9 that of $f(t)$, in accordance with Eq. (16). In SD FROG the FODM has a curvature of $-2/9$ that of $f(t)$, again in accordance with the third time of Eq. (18). In SHG FROG the FODM curvature is 1/2 that of $f(t)$, as the second term of Eq. (20) predicts. Thus, we see that it is straightforward to read the amount of temporal cubic phase directly from the FROG trace.

SPECTRAL CUBIC PHASE

Spectral cubic phase distortion is commonly encountered when one is trying to compress pulses to very short lengths.[29–34] In this case we describe the electric field in the frequency domain as

$$\tilde{E}(\omega) = \exp\left(-\frac{\omega^2}{4a} + id\omega^3\right). \tag{27}$$

For our example (Fig. 7) we chose d such that $d = \tau_{FW}{}^3/2.6$, where τ_{FW} is related to a through Eq. (22). The spectral cubic phase has the characteristic that high and low frequencies acquire more delay than intermediate frequencies, so that the group delay as a function of time is parabolic. In the time domain such a pulse has intermediate frequencies in the leading edge and center but both high and low frequencies in the trailing edge, leading to a beating phenomenon, i.e., the familiar satellite pulses in the time domain [as seen in the inset of Fig. 7(d)].

In Figs. 7(a)–7(c) we see the FROG traces for a pulse with spectral cubic phase. The PG FROG trace nicely shows a parabolic feature, with high and low frequencies exhibiting larger time delays than the intermediate frequencies. The SD FROG trace is similar but reflected about the delay axis (owing to the complex nature of the gate). The SHG FROG trace also shows a clear parabolic feature, but because the SHG FROG trace is always symmetric in delay, the parabolic feature extends to both sides of the trace. Thus, in SHG FROG, one cannot tell the sign of spectral cubic phase, which is yet another manifestation of the temporal ambiguity.

In Fig. 7(d) we plot the group delay as a function of time, $t(f)$, defined analogously to Eq. (14) as $d\phi/df$, as well as the first-order frequency marginal, defined in a manner analogous to Eq. (15). The FROG traces for spectral cubic phase mirror the $t(f)$ curve. This case illustrates another convenient feature of the FROG trace: even though FROG is in principle a time-domain technique, it is equally able to capture the important features of a frequency-domain phase distortion, as is shown in Fig. 7.

The relationship between $t(f)$ and the first-order frequency marginal varies with the amount of spectral cubic phase distortion. It appears therefore that we cannot easily extract quantitative information directly from the FROG trace in the case of spectral cubic phase without the use of the pulse-retrieval algorithm.

DOUBLE PULSE

In the case of double pulsing, FROG can be used to immediately extract the separation and relative phase of the two pulses. Knowledge of the relative phase is essential in experiments involving phase-related pulses.[35,36] We write the double-pulse electric field as

$$E(t) = \exp(-at^2) + B\exp[-a(t-\Delta t)^2 + i\omega_0\Delta t], \quad (28)$$

where B determines the ratio of the pulse heights, Δt is the pulse separation, and ω_0 is the carrier frequency of the pulse. As in conventional autocorrelation, a double pulse produces a FROG trace with three distinct features: one at zero time delay and one each at $\pm\Delta t$. The zero-time-delay feature is a coherent superposition of two of the spots, in which in the FROG trace—unlike conventional autocorrelation—interference occurs. Since the temporal shift corresponds to a linear phase in the frequency domain, this coherent superposition gives fringes in the frequency direction in the FROG trace, as seen in Fig. 8. These fringes are consistent with the known spectrum of a double pulse, which consists of fringes.

The sequence of pulses shown in Fig. 8 shows the PG FROG traces for two different pulse spacings Δt of the two pulses but with the relative phase fixed at zero. The SD and the SHG FROG traces are extremely similar and are not shown here. The spacing of the fringes, Δf, and the separation of pulses, Δt, are related by the simple formula $\Delta f\Delta t = 1$. Thus we can use both the fringe spacing and the spot separation of the FROG trace to determine the pulse separation.

PG and SD FROG can also be used to measure the relative phase of the two pulses. This information is encoded in the phase of the fringes. In Fig. 9 we show the PG FROG trace of a double pulse in which the two pulses are π rad out of phase. The phase of the fringes in the FROG trace is also shifted by π rad. In general the fringes in the FROG trace shift to lower frequencies by an amount equal to the phase shift of the second pulse [$\omega_0\Delta t$ in Eq. (28)]. (In SHG FROG the phase of the fringes does not change, and thus it is difficult to determine the relative phase directly from the SHG FROG trace.) Even if the pulses are linearly chirped or self-phase modulated, the fringes occur near the center of the trace where the two spots overlap, even though the spots themselves are tilted or curved. Thus PG and SD FROG provide a simple way to measure the relative phase of two separated pulses, a task that is otherwise quite difficult.

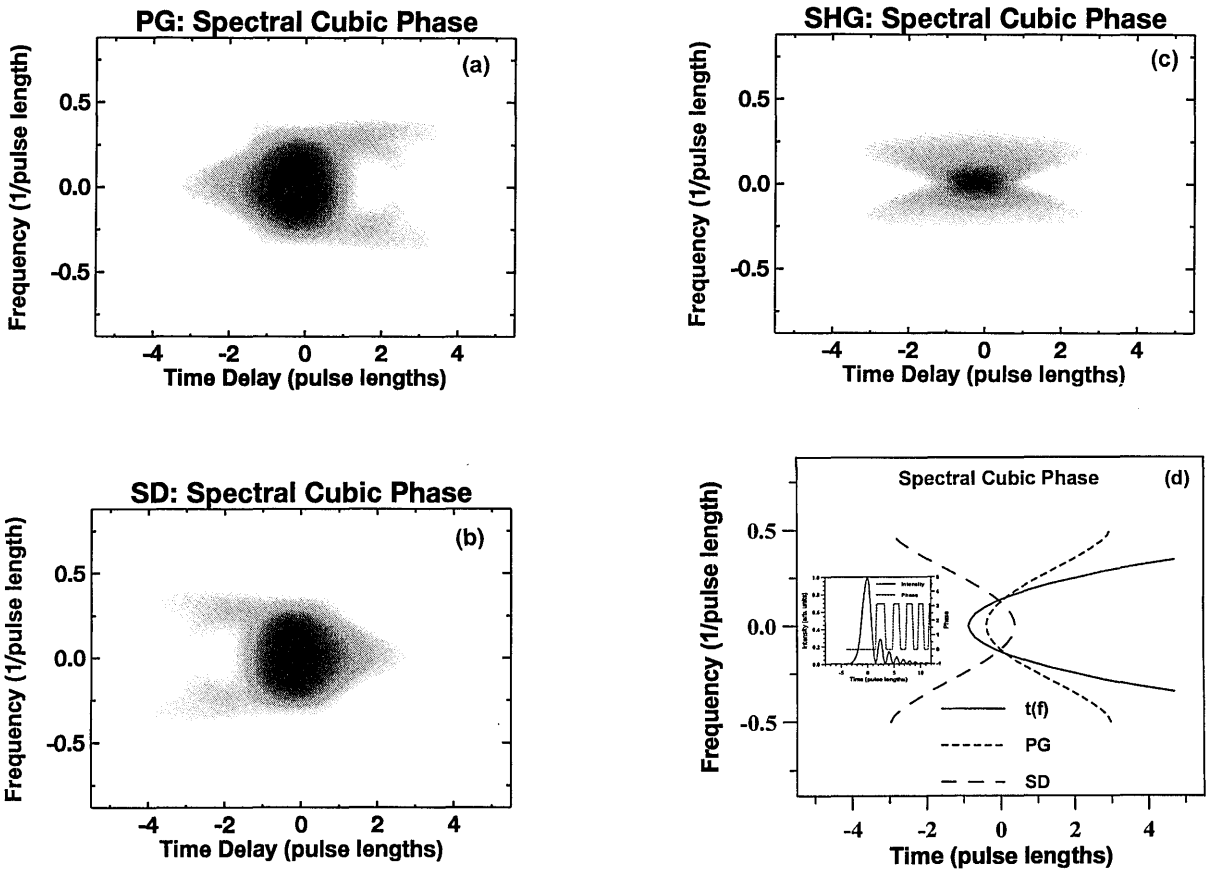

Fig. 7. (a)–(c) The FROG traces of a pulse with spectral cubic phase distortion mirrors the group time delay. The SHG FROG trace is symmetrical about the τ axis, and thus the sign of the cubic phase is ambiguous. (d) The group delay as a function of frequency $t(f)$, and the first-order frequency marginal of the FROG traces. The intensity as a function of time (inset) exhibits a beating phenomenon.

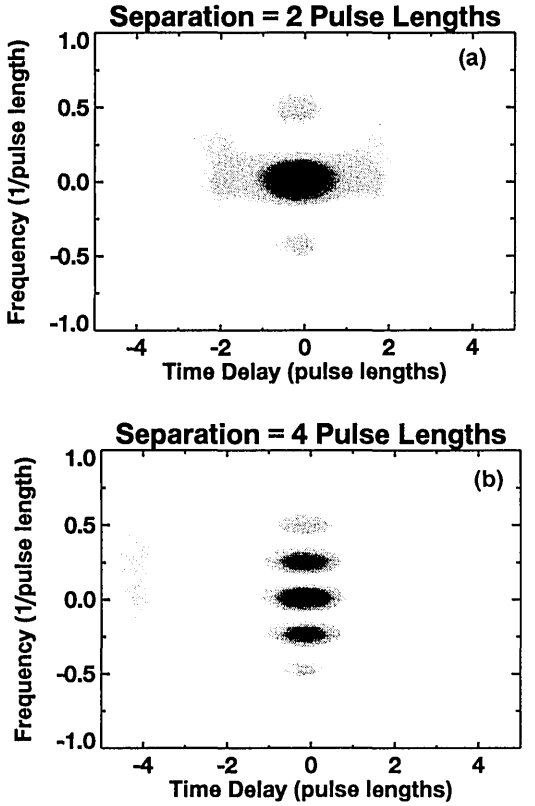

Fig. 8. The PG FROG traces of two pulses of equal amplitude separated by times Δt of (a) 2 and (b) 4 pulse widths. As the pulses move apart, the frequency of the fringes in the f direction becomes higher. The separation of the two pulses is encoded not only in this fringe spacing but also in the separation of the two lower-intensity spots at $\pm\Delta t$. The SD and the SHG FROG traces are similar.

PULSE COMPRESSION: SIMULTANEOUS SELF-PHASE MODULATION AND GROUP-VELOCITY DISPERSION

There are many cases of interest in which the phenomena of SPM and GVD occur at the same time.[27] A soliton (which can occur in an optical fiber in the negative GVD regime) is one of these cases, but because a soliton is a transform-limited pulse, its FROG trace bears no remarkable features and is easily recognized. As a result this case requires no additional discussion.

In the positive GVD regime, where optical fibers are used to broaden and chirp a pulse before compression with a grating pair, the pulse emerging from the fiber has a complex structure. The pulse characteristics in this case are best described in soliton units. We choose to consider a pulse that results from propagation of 0.2 soliton length after beginning with an amplitude of 7 soliton units (note that this pulse propagates in the presence of positive GVD, so it is not a soliton; however, the equation describing the propagation can be scaled in an manner identical to that in the soliton case).

The FROG traces of this positively chirped pulse are shown in Fig. 10(a)–10(c), and in PG and SD FROG they exhibit the positive-slope characteristic of a positively chirped pulse. This pulse, however, shows much more structure than a simple linearly chirped pulse [compare with Fig. 3(a)]. Note that the SD FROG trace has twice the slope of the PG FROG trace, as for pure linear chirp. The SHG FROG trace also exhibits considerable structure but, as expected, shows a zero slope.

In a pulse compressor this pulse can be compressed with relatively high efficiency by application of the proper amount of negative GVD. In Fig. 10(d) we see the PG FROG trace of the pulse after compression with negative GVD (the SD and SHG traces are similar). The amount of GVD was determined from the slope of the $f(t)$ curve for this pulse. The resultant compressed pulse is shorter than the input pulse by a factor of roughly 6. The FROG trace seems to spread a small amount near its upper and lower extremes. Recalling the spectral cubic phase case, we see that the presence of these dissimilar frequencies at the leading and trailing edges of the pulse leads to the well-known small satellite pulses, indicative of imperfect compression of the pulse caused by nonlinear phase distortion. If the incorrect amount of GVD compensation were used to compress the pulse, then some tilt, as well as some structure, would remain in the FROG trace. The direction of tilt would indicate whether too much or too little GVD compensation was used. FROG thus provides an excellent diagnostic for pulse-compression studies.

LINEAR CHIRP AND SPECTRAL CUBIC PHASE

Another pair of phase distortions that often appear together are linear chirp and spectral cubic phase distortion. When chirped pulse amplification is used, for example, if the compressor is not adjusted properly, substantial amounts of both of these phase distortions can be introduced into the pulse. A pulse of this sort was recently diagnosed by use of PG FROG.[37] The FROG traces of a pulse with these two phase distortions present simultaneously are shown in Figs. 11(a)–11(c). The traces look similar to the traces for pure spectral cubic phase [Figs. 7(a)–7(c)] but with a slight asymmetry that is due to the presence of the linear chirp.

The amount of linear chirp in this pulse is quite substantial; b from Eq. (24) is chosen to triple the bandwidth of the pulse over the transform limit ($b = \sqrt{8}\,a$). The

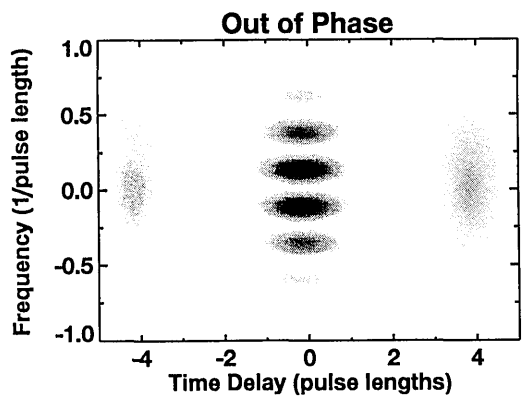

Fig. 9. PG FROG trace for two pulses of equal amplitude separated by 4 pulse widths and out of phase. The trace is similar to that of Fig. 8(b) except that the fringes along the zero time delay axis are also shifted out of phase. The phase shift of the fringes can be used to measure the relative phase separation of the two pulses.

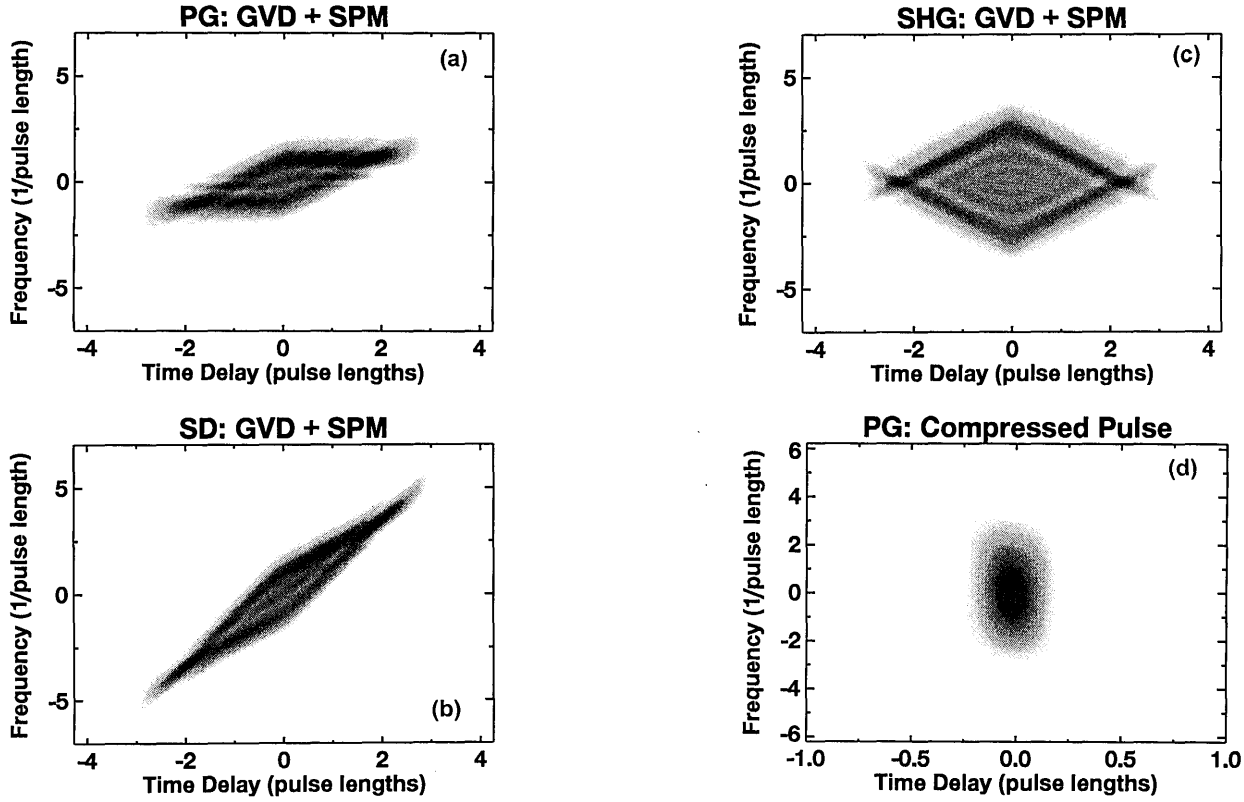

Fig. 10. (a)–(c) FROG traces of a pulse after it has undergone SPM and positive GVD in a fiber. The pulse had an amplitude of 7, and the fiber was 0.2 unit long, both measured in soliton units. The spectrum (not shown) of the pulse has a four-peaked structure. The SD FROG trace has twice the slope as the PG FROG trace, as in linear chirp, while the SHG FROG trace again has no slope. (d) PG FROG trace of the same pulse as (a) after the pulse has undergone negative GVD compensation. The pulse width is roughly one sixth of its original length. The flaring out seen at high and low frequencies is evidence of imperfect compression and leads to the well-known satellite pulses in the time domain (see text).

spectral cubic phase coefficient is $d = \tau_{FW}{}^3/34.3$, as defined in Eq. (27). This amount of spectral cubic phase is quite small; in the absence of linear chirp, the temporal intensity profile of the pulse does not exhibit any visible satellite pulses. However, the addition of linear chirp causes the pulse to acquire several substantial satellite peaks, as shown in Fig. 11(d). Thus we see that the presence of linear chirp amplifies the effects of spectral cubic phase.

The FROG trace, too, reflects this fact. When only linear chirp is present, the FROG traces of this pulse look like those in Fig. 3. When only the spectral cubic phase is present, the FROG traces look almost like those of a transform-limited pulse. Therefore a visual inspection of the FROG trace would be useful when, for example, a pulse compressor is being adjusted for minimum spectral cubic phase. The linear chirp can be increased to magnify the effects of spectral cubic phase, the cubic phase minimized, and then the linear chirp minimized to give the best possible compression.

Another characteristic feature of the combination of linear chirp and cubic spectral phase is evident in the PG and the SD FROG traces. There are fringes in the FROG trace near zero delay and at large and small frequencies. These fringes are not present when only linear chirp or several cubic phase are present and therefore are indicative of the combination of these two phase distortions.

PHASE JUMPS

It is also interesting to consider the case of a pulse with a smooth intensity envelope but with an abrupt phase jump, that is, constant phase φ_0 for times $t < 0$ and then a jump to a new constant-phase value, φ_0', for times $t > 0$. The PG and the SD FROG traces for a pulse with a phase jump of $\varphi_0 - \varphi_0' = \pi$ at pulse center are identical and are shown in Fig. 12. The SHG FROG trace (not shown) is similar but with a bright spot, rather than a dark spot, in the center. These traces are best understood by thinking of them as double-pulse traces, with the pulses having less separation that those considered above. The central regions in the trace of Fig. 12 show a similar type of interference as in the double pulse traces.

INTENSITY SUBSTRUCTURE

Figures 13(a) shows a pulse with complex intensity and phase structure. The PG FROG trace of this pulse, shown in Fig. 13(b), reveals this complexity. (The SD and the SHG FROG traces are quite similar in their complexity, although of course the SHG FROG trace is symmetric about the $\tau = 0$ axis.) If the pulse had a flat phase, the FROG trace would be symmetric about the $f = 0$ axis. Note that there is considerable structure in the FROG trace, indicative of the considerable structure in the pulse intensity and the phase profiles. Although

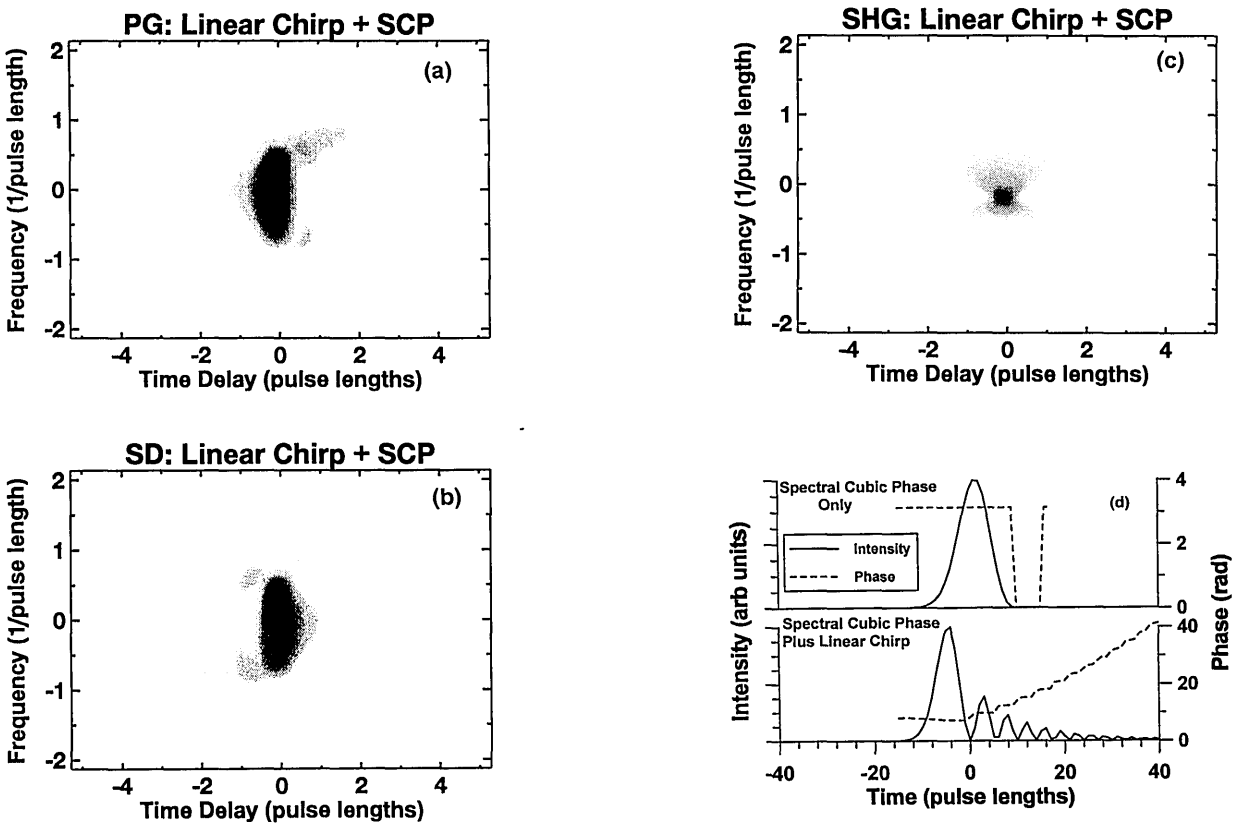

Fig. 11. (a)–(c) FROG traces of a pulse with linear chirp and spectral cubic phase. The traces resemble the traces for pure spectral cubic phase but with an asymmetry induced by the presence of linear chirp. (d) Intensity and phase profiles of a pulse with a small amount of spectral cubic phase and with a combination of spectral cubic phase and linear chirp. The amount of spectral cubic phase is the same in both pulses. The addition of linear chirp amplifies the effect of the spectral cubic phase considerably.

obtaining the details of the pulse substructure requires running the iterative algorithm, it would be difficult to misidentify a pulse with significant intensity (or phase) substructure from its FROG trace.

EXPERIMENTAL EXAMPLE

We now show an example of reading phase information about the pulse directly from an experimental FROG trace. Figure 14(a) shows an experimental PG FROG trace. This trace was discussed in detail in Ref. 28. The pulse exhibits some positive slope, which is indicative of positive linear chirp. There is also a slight curvature to the trace, which indicates temporal cubic phase. Using a only a ruler and pencil, we estimate the slope of the trace to be $b = 5.6 \times 10^{-6}$ fs^{-2}, where $\omega(\tau) = b\tau$, and the curvature of the trace (after subtracting out the linear slope) to be $c = 1.6 \times 10^{-8}$ fs^{-3}, where $\omega(\tau) = c\tau^2$. After applying the scaling factors as determined by Eq. (16), we can construct an estimate for the phase of the pulse. In Fig. 14(b) we show the intensity and the phase extracted by the FROG pulse retrieval algorithm as well as the phase constructed with the values cited above (dashed curve). Although the agreement is not perfect, it is reasonable, given the complexity of the structure of this pulse. On pulses with simpler structure the technique will perform even more accurately.

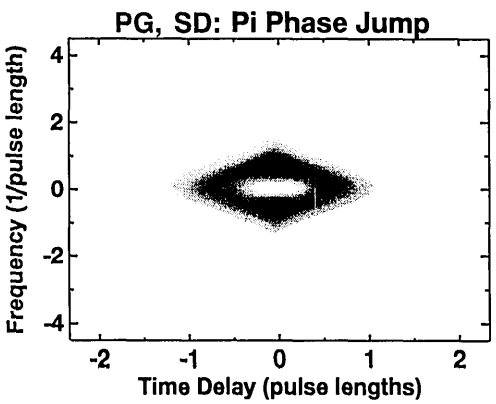

Fig. 12. PG FROG trace of a pulse with a phase jump of π at pulse center and a Gaussian intensity profile. The SD FROG trace of this pulse is identical.

CONCLUSION

Frequency-resolved optical gating (FROG), a simple and convenient technique for fully characterizing ultrashort pulses, also produces an intuitive trace: a type of spectrogram of a single pulse. Although a phase-retrieval algorithm is necessary to extract exact information about the phase and amplitude of the pulse, one can gain much insight immediately by a simple visual inspection of the FROG trace. This is because the FROG trace often gives a close approximation to the instantaneous frequency as a function of time, $f(t)$, as well as directly displaying the

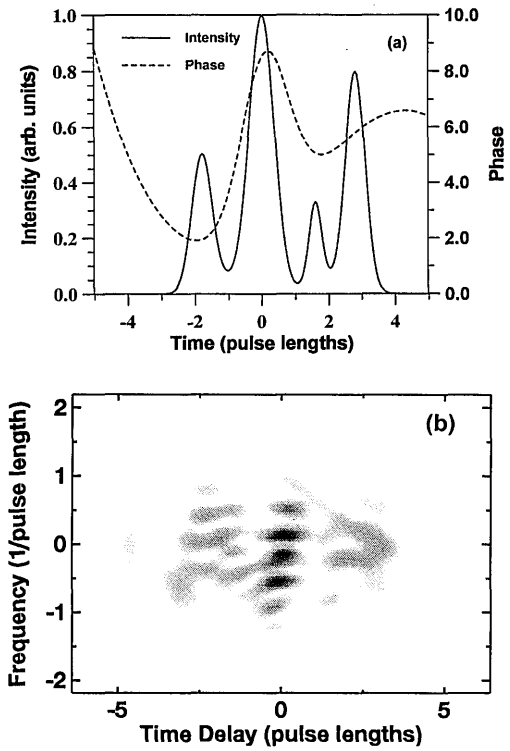

Fig. 13. (a) Pulse with a complicated intensity and phase profile. (b) PG FROG trace of the same pulse. The SD and the SHG FROG traces show similar levels of complexity.

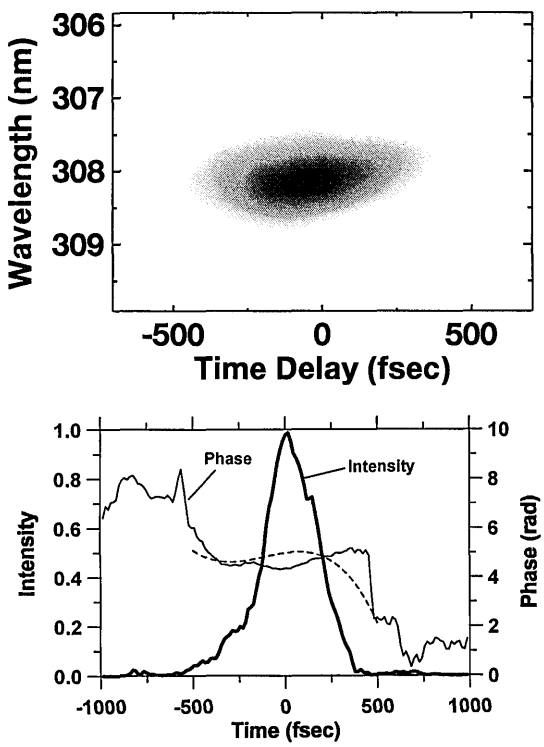

Fig. 14. (a) PG FROG trace of a pulse exhibiting positive linear chirp and temporal cubic phase. (b) Pulse intensity and phase derived from the FROG trace of (a), as well as an estimate (dashed curve) of the phase generated from a visual inspection of the trace. Agreement is good, considering the complicated structure of the pulse.

(approximate) temporal and spectral widths of the pulse. The availability of this information in a visual, real-time display is a great advantage for experimentalists working with ultrashort pulses.

Several experimental geometries can be used to generate the FROG trace. In this investigation we concentrated on the three most common geometries: polarization gate, self-diffraction, and second-harmonic generation. The qualitative and quantitative details of the FROG trace vary considerably among the various geometries.

One can extract quantitative information from a visual inspection of the FROG trace. In this paper we have provided the proper scaling factors necessary to do this for various types of phase distortion. If only one type of phase distortion exists in the pulse, this sort of quantitative estimation may be possible, but in general it is much safer to use the pulse-retrieval algorithm to obtain quantitative values.

While the mathematical algorithm required for full pulse retrieval is not difficult and generally converges quickly,[11,16] good intuition as to the characteristics of the FROG trace are nevertheless helpful for its use. In this paper we have provided a sampler of FROG traces for the various FROG geometries and for a variety of representative pulse distortions, including linear chirp, spectral and temporal cubic phase, self-phase modulation (SPM), double pulsing, a combination of group-velocity dispersion and SPM, phase jumps, and pulses with significant intensity substructure. With this catalog it should be possible to recognize a wide range of pulses almost immediately.

REFERENCES AND NOTES

1. J. A. Giordmaine, P. M. Rentzepis, S. L. Shapiro, and K. W. Wecht, "Two-photon excitation of fluorescence by picosecond light pulses," Appl. Phys. Lett. **11,** 216–218 (1967).
2. E. P. Ippen and C. V. Shank, *Ultrashort Light Pulses—Picosecond Techniques and Applications*, S. L. Shapiro, ed. (Springer-Verlag, Berlin, 1977), p. 83.
3. S. M. Saltiel, K. A. Sankov, P. D. Yankov, and L. I. Telegin, "Realization of a diffraction-grating autocorrelator for single-shot measurement of ultrashort light pulse duration," Appl. Phys. B **40,** 25–27 (1986).
4. J.-C. M. Diels, J. J. Fontain, I. C. McMichael, and F. Simoni, "Control and measurement of ultrashort pulse shapes (in amplitude and phase) with femtosecond pulses," Appl. Opt. **24,** 1270–1282 (1985).
5. K. Naganuma, K. Mogi, and H. Yamada, "General method for ultrashort pulse chirp measurement," IEEE J. Quantum Electron. **25,** 1225–1233 (1989).
6. J. L. A. Chilla and O. E. Martinez, "Direct determination of the amplitude and the phase of femtosecond light pulses," Opt. Lett. **16,** 39–41 (1991).
7. D. Marcuse and J. M. Weisenfeld, "Chirped picosecond pulses: evaluation of the time-dependent wavelength for semiconductor film lasers," Appl. Opt. **23,** 74–82 (1984).
8. J.-C. Diels, X. M. Zhao, and S. Diddams, "Capturing electromagnetic fields with fs resolution," in *Ultrafast Pulse Generation and Spectroscopy*, T. R. Gosnell and A. J. Taylor, eds., Soc. Photo-Opt. Instrum. Eng. **1861,** 120–130 (1993).
9. V. Wong, J. Koshel, M. Beck, and I. Walmsley, "Measurement of the amplitude and phase of pulses from passively modelocked lasers," in *Ultrafast Pulse Generation and Spectroscopy*, T. R. Gosnell and A. J. Taylor, eds., Soc. Photo-Opt. Instrum. Eng. **1861,** 137–148 (1993).
10. D. J. Kane and R. Trebino, "Characterization of arbitrary femtosecond pulses using frequency-resolved optical gating," IEEE J. Quantum Electron. **29,** 571–579 (1993).

11. R. Trebino and D. J. Kane, "Using phase retrieval to measure the intensity and phase of ultrashort pulses: frequency-resolved optical gating," J. Opt. Soc. Am. A **10,** 1101–1111 (1993).
12. D. J. Kane and R. Trebino, "Single-shot measurement of the intensity and phase of an arbitrary ultrashort pulse by using frequency-resolved optical gating," Opt. Lett. **18,** 823–825 (1993).
13. W. Koenig, H. K. Dunn, and L. Y. Lacy, "The sound spectrograph," J. Acoust. Soc. Am. **18,** 19–49 (1946).
14. L. Cohen, "Time-frequency distribution," Proc. IEEE **77,** 941–981 (1989).
15. R. A. Altes, "Detection, estimation, and classification with spectrograms," J. Acoust. Soc. Am. **67,** 1232–1246 (1980).
16. K. W. DeLong and R. Trebino, "Improved ultrashort pulse-retrieval algorithm for frequency-resolved optical gating," J. Opt. Soc. Am. A **11,** 2429–2437 (1994).
17. E. B. Treacy, "Measurement and interpretation of dynamic spectrograms of picosecond light pulses," J. Appl. Phys. **42,** 3848–3858 (1971).
18. A. Freiberg and P. Saari, "Picosecond spectrochronography," IEEE J. Quantum Electron. **QE-19,** 622–630 (1983).
19. J. Paye, "The chronocyclic representation of ultrashort light pulses," IEEE J. Quantum Electron. **28,** 2262–2273 (1992).
20. J. Paye, M. Ramaswamy, J. G. Fujimoto, and E. P. Ippen, "Measurement of the amplitude and phase of ultrashort light pulses from spectrally resolved autocorrelation," Opt. Lett. **18,** 1946–1948 (1993).
21. K. DeLong, R. Trebino, and W. E. White, "Frequency-resolved optical gating using second-harmonic generation," submitted to J. Opt. Soc. Am. B.
22. D. J. Kane and R. Trebino, U.S. Patent Application Serial Number 07/966,644 (October 26, 1992).
23. R. DeSalvo, D. J. Hagan, M. Sheik-Bahae, G. Stegeman, E. W. Van Stryland, and H. Vanherzeele, "Self-focusing and self-defocusing by cascaded second-order effects in KTP," Opt. Lett. **17,** 28–30 (1992).
24. The FROG trace of this transform-limited pulse is an ellipse (or circle) oriented along either axis, depending on the width of the pulse. The trace will be circular when the pulse width $\tau_{FW} = 0.79\sqrt{N}$ for PG and SD FROG and $\tau_{FW} = 0.66\sqrt{N}$ for SHG FROG, where N is the number of elements in the fast Fourier transform used to generate the FROG trace. The fast Fourier transform relates the scaling of the two axes through $\delta f = 1/(N\delta\tau)$ [W. H. Press, W. T. Vetterling, and S. A. Teukolsky, *Numerical Recipes in C: Second Edition* (Cambridge U. Press, Cambridge, 1992)], where δf and $\delta\tau$ are the increments of frequency and delay in the fast Fourier transform.
25. A. E. Siegman, *Lasers* (University Science, Mill Valley, Calif., 1986), Chap. 9.
26. K. W. DeLong and J. Yumoto, "Chirped light and its characterization using the cross-correlation technique," J. Opt. Soc. Am. B **9,** 1593–1604 (1992).
27. G. P. Agrawal, *Nonlinear Fiber Optics* (Academic, San Diego, 1989).
28. D. J. Kane, A. J. Taylor, R. Trebino, and K. W. DeLong, "Single-shot measurement of the intensity and phase of femtosecond UV laser pulse," Opt. Lett. **8,** 1061–1063 (1994).
29. R. L. Fork, C. H. Brito Cruz, P. C. Becker, and C. V. Shank, "Compression of optical pulses to six femtoseconds by using cubic phase compensation," Opt. Lett. **12,** 483–485 (1987).
30. C. P. J. Barty, B. E. Lemoff, and C. L. Gordon III, "Generation, measurement, and amplification of 20-fsec high-peak-power pulses from a regeneratively initiated self-modelocked Ti:sapphire laser," in *Ultrafast Pulse Generation and Spectroscopy*, T. R. Gosnell and A. J. Taylor, eds., Soc. Photo-Opt. Instrum. Eng. **1861,** 6–30 (1993).
31. M. T. Asaki, C.-P. Huang, D. Garvey, J. Zhou, M. M. Murname, and H. C. Kapteyn, "Generation and amplification of sub-20-femtosecond pulses in Ti:sapphire," in *Ultrafast Pulse Generation and Spectroscopy*, T. R. Gosnell and A. J. Taylor, eds., Soc. Photo-Opt. Instrum. Eng. **1861,** 37–41 (1993).
32. W. E. White, F. G. Patterson, L. D. V. Woerkom, D. F. Price, and R. L. Shepherd, "Limitations on the fidelity of 100 fsec pulses produced by chirped-pulse amplification," in *Ultrafast Pulse Generation and Spectroscopy*, T. R. Gosnell and A. J. Taylor, eds., Soc. Photo-Opt. Instrum. Eng. **1861,** 55–60 (1993).
33. M. Stern, J. P. Heritage, and E. W. Chase, "Grating compensation of the third-order fiber dispersion," IEEE J. Quantum Electron. **28,** 2742–2748 (1992).
34. J. M. Jacobsen, K. Naganuma, H. A. Haus, J. G. Fujimoto, and A. G. Jacobsen, "Femtosecond pulse generation in a Ti:AlO laser by using second- and third-order intracavity dispersion," Opt. Lett. **17,** 1609–1610 (1992).
35. J. T. Fourkas, W. L. Wilson, G. Wackerle, A. E. Frost, and M. D. Fayer, "Picosecond time-scale phase-related optical pulses: measurement of sodium optical coherence decay by observation of incoherent fluorescence," J. Opt. Soc. Am. B **6,** 1905–1910 (1989).
36. S. A. Rice, "New ideas for guiding the evolution of a quantum system," Science **258,** 412–413 (1992).
37. B. Kohler, J. L. Krause, F. Raski, C. Rose-Petruck, R. M. Whitnell, K. R. Wilson, V. V. Yakovlev, and Y. J. Lam, "Quantum control with tailored femtosecond pulses," presented at OE/LASE 94 (Society of Photo-Optical Instrument Engineers, Los Angeles, 1994), presentation 2116-55.